

# Electron energy transport inferences from modulated electron cyclotron heating in DIII-D

K. W. Gentle and M. E. Austin

*Fusion Research Center, University of Texas, Austin, Texas 78712*

J. C. DeBoo, T. C. Luce, and C. C. Petty

*General Atomics, San Diego, California 92186*

(Received 4 October 2005; accepted 12 December 2005; published online 27 January 2006)

Electron thermal energy transport in high-temperature plasmas is poorly understood. A useful characterization of the transport as energy flux versus temperature gradient may be obtained for a modest range of fluxes and gradients about an equilibrium by using modulated electron cyclotron heating. The transport is rapid and stiff (high  $\chi_{\text{inc}}$ ) at the outside, becoming slower and more diffusive toward the center. © 2006 American Institute of Physics. [DOI: 10.1063/1.2163251]

## I. INTRODUCTION

Modulated electron cyclotron heating (ECH) is a powerful technique for exploring electron thermal transport. By averaging over many modulation periods, the electron temperature response to change in heating can be determined with great precision and subjected to careful analysis. The temperature data are generally Fourier analyzed and the amplitude and phase from one or more harmonics compared with a model calculation.<sup>1</sup> The model diffusivity  $\chi_e(r)$  is chosen for the best fit to the observations. This is a versatile technique that may be applied to almost any data set, and it has been applied on many devices.<sup>2-5</sup> However, the conclusions are model dependent, and it may be difficult to fit both amplitude and phase with one choice of  $\chi_e(r)$ .

The realization of complete electron temperature profiles with high spatial and temporal resolution from electron cyclotron emission (ECE)<sup>6</sup> makes possible a direct transport analysis that obviates the use of models and provides the radial electron heat flux  $Q_e(r, t)$  as a function of the temperature gradient  $\nabla T_e(r, t)$  over the modulation cycle. This formulation, flux as a function of gradient, offers a more natural comparison with the results of theory and computer simulations of turbulence and transport. The transport analysis is also “self-calibrating” in the sense that it provides an independent measure of the ECH power absorbed by the plasma that may be compared with calorimetric measures of power to the antenna.

Section II discusses the methods and procedures of the analysis, and Sec. III presents results for the total power absorbed by the electrons and related questions of system linearity, which suggest that a  $\chi_e(r)$  may not be a good characterization of the plasma. Section IV treats the observations of  $Q_e(r, t)$  as a function of  $\nabla T_e(r, t)$  for a variety of conditions. The conclusions are summarized in Sec. V.

## II. METHOD OF ANALYSIS

The transport analysis is conventional. The heat flux is obtained from energy conservation with the usual expression

$$Q_e = \frac{1}{r} \int_0^r r dr \left[ q_e(r, t) - \frac{\partial(3/2nT_e)}{\partial t} \right], \quad (1)$$

where  $q_e(r, t)$  is the net power to the electrons including Ohmic, beam, and ECH inputs, radiation losses, and transfer to the ions. The contribution to  $q_e(r, t)$  from the modulated ECH is discussed in detail below; the other terms are calculated from a transport code—ONETWO (Ref. 7) in these cases. Since ONETWO is time independent, the terms represent the average over the modulation cycle. The two terms in  $q_e(r, t)$  that are sensitive to the electron temperature variations over the cycle are the Ohmic heating and the electron-ion exchange. These terms are modulated about their average value using the measured  $T_e(r, t)$ . The current density is assumed “frozen” on the time scale of the modulation in calculating the Ohmic deposition. The ion temperature modulation has been observed to be much less than the electron modulation and is assumed constant for the electron-ion energy exchange. The density is also assumed constant, consistent with observations. In practice, the modulation of the Ohmic power is rarely significant because the Ohmic power is usually small compared with the auxiliary heating power. Similarly, the modulation of the electron-ion exchange is often not significant because with strong beam heating, the electron temperature modulation is fractionally small. The modulated ECH is always the dominant modulation in  $q_e(r, t)$ .

The analysis requires some care, because the effects of noise are greatly magnified by the time derivative of the electron temperature. Averaging over many (ten or more) modulation periods provides data of sufficient quality. All data shown here are the result of multiperiod boxcar averaging, omitting the initial one or two periods before periodicity is established. A great advantage of this method of transport analysis is that the flux of Eq. (1) is determined as an integral. Integrals are robust to small errors in the integrand.

An additional subtlety involves  $T_e(r, t)$ . The analysis of Eq. (1) is based on a fixed, approximate cylindrical geometry. However, the ECE channels are a set of  $T_e(R, t)$ , with  $R$  determined by the receiver frequency and the (fixed) total magnetic-field strength. The conversion  $r(R)$  uses the actual magnetic geometry as determined from EFIT, but in cases of

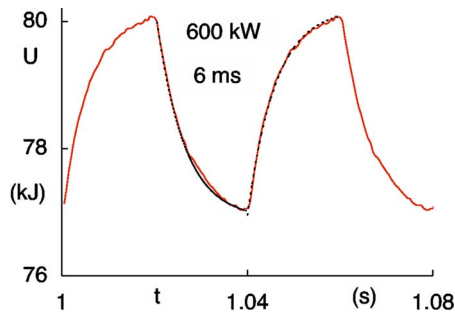


FIG. 1. (Color online) Total electron energy  $U(t)$  for the averaged response to modulated ECH for deposition at  $\rho=0.6$  into an  $L$  mode at 800 kA with 4 MW NBI and average density of  $2.5 \times 10^{19} \text{ m}^{-3}$ . The dashed line is an exponential fit with a time constant of 6 ms and amplitude corresponding to 600 kW of modulated power from Eq. (5).

strong ECH heating near the center, the magnetic geometry changes slightly over the modulation cycle, leading to an  $r(R, t)$ . In these cases, the  $T_e(R, t)$  are interpolated to produce the set  $T_e(r, t)$  at a set of fixed minor radii for the transport analysis. The variation in  $\rho=r/a$  never exceeds a few percent.

The physics of ECH has been extensively studied (see the recent review by Prater<sup>8</sup>). The contribution to  $q_e(r, t)$  from the modulated ECH power may be evaluated in several ways. The power to the antenna is measured by calorimetry. The deposition profile is calculated by TORAY.<sup>9</sup> To avoid details of the radial deposition profile within the narrow resonance layer, the analysis of Eq. (1) is not applied to this region. It is applied either to radii inside the deposition region, for which there should be no modulated ECH power, or to radii outside the deposition region, for which the radial integral should include all the modulated ECH power. An alternative inference of the total power deposition may be obtained from measurements of the total electron thermal energy,

$$U_e(t) = \int_0^a \frac{3}{2} n T_e r dr. \quad (2)$$

For square-wave modulation, the rate of change,  $dU_e/dt$ , at turn-on and turn-off implies a power deposition. The specific calculation is discussed in Sec. III.

The experiments were conducted in DIII-D (Ref. 10) using a multimewatt gyrotron system for ECH.<sup>11</sup> For the past several years of operation, the power inferred from  $U_e(t)$  has agreed within 20% with the value from ECH calorimetry.

### III. POWER DEPOSITION AND SYSTEM LINEARITY

Figure 1 shows a representative plot of  $U_e(t)$  in response to a square-wave ECH modulation. The dashed lines are best-fit exponential decays to the new equilibrium. The system clearly looks as if it were approaching each of the equilibria, no ECH or full ECH, with a characteristic exponential time constant. One is therefore led to describe the plasma with a simple zero-dimensional (0D) model for the modulation of  $U$ :

$$\frac{dU_{\text{mod}}}{dt} = P_{\text{mod}}(t) - \frac{U_{\text{mod}}}{\tau}, \quad (3)$$

where  $P_{\text{mod}}$  is the ECH power  $P_{\text{ECH}}$  when it is on and 0 when off,  $\tau$  is the exponential decay time, and  $T$  will be the duration of the on and off portions of the cycle. The solutions have the form

$$\text{On: } U_{\text{mod}}(t) = \tau P_{\text{ECH}} - U_1 e^{-t/\tau},$$

$$\text{Off: } U_{\text{mod}}(t) = U_2 e^{-t/\tau}. \quad (4)$$

Continuity at the switching times  $T$  requires

$$U_1 = U_2 = U_m = \frac{\tau P_{\text{ECH}}}{1 + e^{-T/\tau}}, \quad (5)$$

where  $U_m$  and  $\tau$  are the parameters fit to the observations as in Fig. 1 and  $P_{\text{ECH}}$  is the implied ECH power. This reduces to the two well-known limiting cases. If the duration  $T$  is long compared with the relaxation time  $\tau$ , the system reaches each of its equilibria and  $P_{\text{ECH}}$  is the maximum value of  $dU/dt$ . If, on the other hand,  $T$  is short compared with  $\tau$ , the system stays near  $U$  given by  $P_{\text{ECH}}/2$  and the effective modulation is only the remaining  $P_{\text{ECH}}/2$ . In this case,  $P_{\text{ECH}}$  approaches twice the maximum value of  $dU/dt$ .

The 0D model of Eq. (3) is a natural consequence of a standard transport equation:

$$\frac{3}{2} n \frac{\partial T}{\partial t} = \frac{1}{r} \frac{\partial}{\partial r} \left( r n \chi \frac{\partial T}{\partial r} \right) + q. \quad (6)$$

If this equation can be linearized for perturbations about the equilibrium solution for fixed  $q(r)$  and  $n(r)$ , the homogeneous equation that follows can be separated with a time dependence  $e^{-t/\tau}$ . The thermal diffusivity  $\chi$  in Eq. (6) may be a nonlinear function of state variables; the only requirement is that it be represented by a simple  $\chi(r)$  in the linear Eq. (7) for the perturbation. The  $\chi$  in Eq. (7) is the  $\chi_{\text{inc}}$  or  $\chi_{\text{HP}}$  value and may differ from the equilibrium power balance value  $\chi_{\text{PB}} = Q_{\text{eq}} / (n_{\text{eq}} dT_{\text{eq}}/dr)$ . The equation for  $T(r)$ ,

$$\frac{\partial}{\partial r} \left( r n \chi \frac{\partial T}{\partial r} \right) + \frac{3}{2} r n \frac{T}{\tau} = 0, \quad (7)$$

is of Sturm-Liouville type with eigenvalues for  $\tau$ . The solutions can therefore be written as

$$T_e(r, t) = \sum_{i=1}^{\infty} c_i T_i(r) e^{-t/\tau_i}, \quad \tau_i > \tau_{i+1}, \quad (8)$$

with orthogonality

$$\int_0^a T_i T_j r n dr = 0, \quad i \neq j. \quad (9)$$

Because of the decreasing  $\tau_i$ , the  $T_e(r, t)$  from Eq. (8) is rapidly dominated by the first term. Furthermore, the similarity of the integral for  $U_e$ , Eq. (2), to the orthogonality condition of Eq. (9) guarantees that  $U_e(t)$  will exhibit only the fundamental time constant  $\tau_1$ . Therefore the simple 0D model of Eqs. (3)–(5) is a natural consequence of any linearized transport with the general form of Eq. (6).

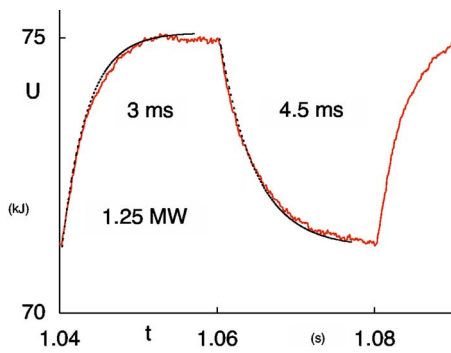


FIG. 2. (Color online) Total electron energy  $U(t)$  for the averaged response to modulated ECH for deposition at  $\rho=0.75$  into an  $L$  mode with the same conditions as in Fig. 1. The dashed lines are exponential fits with an amplitude corresponding to 1.25 MW of modulated power from Eq. (5) and time constants as indicated.

These features are easily demonstrated for constant  $n$  and  $\chi$ , for which Eq. (7) may be solved analytically in terms of Bessel functions. They have also been confirmed with numerical solutions for realistic  $n(r)$  and  $\chi(r)$ , modulation frequencies, and for various deposition radii  $q(r)$ .

However, the prediction of a single  $\tau$  for all cases in a linear model is not confirmed experimentally. A number of deviations from the predictions of a linear model are observed. One example is shown in Fig. 2, for which relaxation times are different for the rise and fall of energy. The magnitude of the energy change is scarcely sufficient to suggest nonlinearity. More significantly, the relaxation times vary with deposition radius for the same ECH power applied to the same initial discharge condition. The observations are tabulated in Table I. From Eqs. (6)–(9), one would expect the amplitude of the perturbation to  $U_e$  to vary with deposition radius, but all perturbations should decay with  $\tau_1$ . An even more dramatic demonstration of nonlinearity is shown in Fig. 3, which shows  $U_e(t)$  for a case of triangular modulation of the ECH power. This power wave form is symmetric about the peak, a symmetry that is preserved by a linear system. The asymmetric delay times for rise and fall of the energy violate this symmetry, giving a definite signature of nonlinearity.

These observations imply that the linearization of Eq. (6) for perturbations about an equilibrium is not an adequate description of modulated ECH experiments. Since this process underlies most conventional models, for example, those used to analyze the Fourier components of the perturbations, problems with such analyses are to be expected.

TABLE I. Dependence of relaxation time on deposition radius.

Deposition radius ( $\rho$ )	Timeconstant(ms)
0.2	13
0.4	9
0.6	6
0.7	4

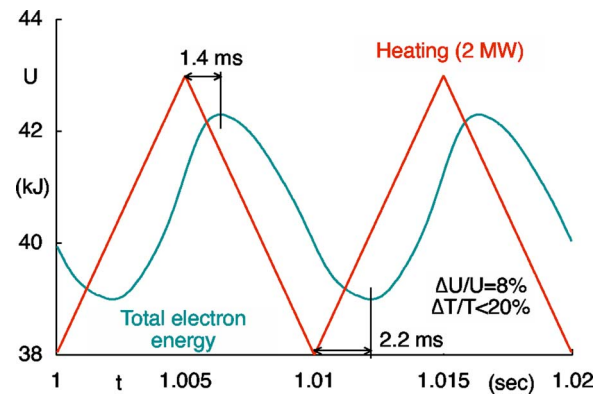


FIG. 3. (Color online) Total electron energy  $U(t)$  for the averaged response to triangle-wave ECH for deposition at  $\rho=0.1$  into an  $L$  mode at 800 kA with 4.7 MW NBI and average density of  $2.5 \times 10^{19} \text{ m}^{-3}$ .

The transport analysis based on Eq. (1), as used in the remainder of this paper, makes no assumption of linearity. The model of Eq. (3) is employed to determine the ECH power absorbed by the plasma for the analysis, but Eq. (3) is justified on strictly empirical evidence as in Fig. 1 and to a good approximation in Fig. 2, the differing rise and decay time constants giving the same estimate of ECH power to within 10%.

#### IV. TRANSPORT MEASUREMENTS

A typical set of  $T_e(\rho, t)$  from a modulated ECH experiment is shown in Fig. 4. For clarity, positions are given in terms of  $\rho=r/a$ . The wave forms are averaged over 14 modulation periods in this case, excluding data from the transient periods at the start of modulation. The zero of  $T_e$  is suppressed to illustrate the modulation. For clarity, not all of the 18 channels are plotted. This is the same discharge as shown in Fig. 1: 500 kW of ECH with a deposition radius of  $\rho=0.6$  and modulated at 25 Hz, applied to a standard  $L$  mode with 4 MW of neutral beam heating. The toroidal field is 2 T, the plasma current is 800 kA, the average density is  $2.5 \times 10^{19} \text{ m}^{-3}$ , and beam heating is applied early to maintain  $q(0) > 1$  and suppress sawteeth for the duration of ECH. The optical depth for the outermost channel shown in Fig. 4 is above 2, the depth at  $\rho=0.83$  is above 3, and the depth in-

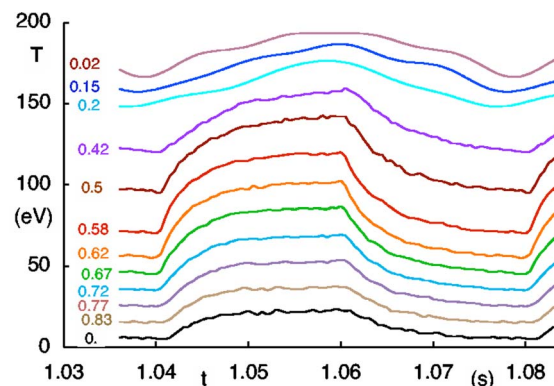


FIG. 4. (Color online) The electron temperature averaged over 14 periods for the case shown in Fig. 1.

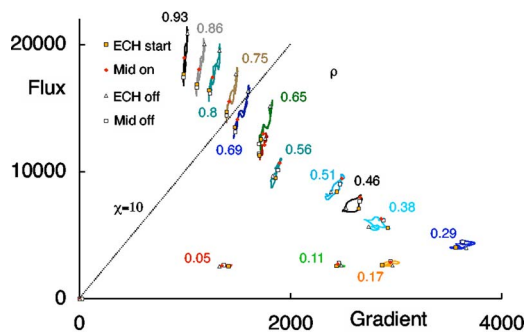


FIG. 5. (Color online) Electron heat flux (per particle) as a function of temperature gradient over a cycle of ECH modulation at various minor radii for the conditions of Fig. 1. Simple diffusivities correspond to trajectories through the origin; an example for  $\chi_e=10$  m<sup>2</sup>/s is shown.

increases rapidly at small radii. The optical depth for the outermost channel used in transport analysis is just above 1. The uniformity of the calibration of ECE with Thomson scattering over radius implies no strong effects of optical depth on the temperature measurements.

The density is monitored by a vertical interferometer chord at  $\rho=0.2$  on the outboard side. Although there is no discernable modulation on the interferometer trace, subjecting the data to the same analysis applied to the temperature data indicates a slight modulation, corresponding to a fractional change of 0.5% at 25 Hz. This should be compared with the fractional temperature modulation of order 5%. The phase difference is close to 90°.

For analysis, the  $T_e(\rho, t)$  are used with Eq. (1) to compute  $Q_e(\rho, t)$ . The data are also differenced to obtain  $\nabla T_e(\rho, t)$ . Both  $Q_e$  and  $\nabla T_e$  are evaluated at the set of  $\rho_i$  between the radii of  $T_e(\rho, t)$ . Time is the parameter to construct the plot of  $Q_e(\nabla T_e)$  at each of the  $\rho_i$ . The result of this analysis for the data of Fig. 4 is shown in Fig. 5. Since there are no easily recognized units for the axes, the gradient is with respect to  $\rho$ , leaving  $\nabla T_e$  in eV, and the flux is rescaled as  $Q_e/n$  in units of eV m<sup>2</sup>/s. As a consequence, the quotient is  $\chi_e$  (m<sup>2</sup>/s) directly. As an example, the  $\chi_e=10$  line is plotted in Fig. 5. To indicate the relation of these trajectories to the original time series, four points from the cycle are marked: the turn-on of ECH (temperature minimum), midpoint of ECH, turn-off of ECH (maximum temperature), and midpoint of zero power interval.

The trajectories of Fig. 5 give a useful characterization of  $Q_e(\nabla T_e)$  over a region of parameter space, at least outside the deposition radius. Inside the deposition radius, the modulation of both flux and gradient becomes small, and the results are less definitive. The trajectories outside  $\rho=0.6$  can be described as line segments with slopes significantly steeper than an equivalent  $\chi_e$ . The largest radii have the steepest slopes. This qualitative behavior has been found in every case for which an analysis has been done, including not only modulated ECH but also sawtooth perturbations.<sup>12</sup> It corresponds to a  $\chi_{inc} \gg \chi_{PB}$ . The steep trajectories cannot be ascribed to optical depth effects. The effect persists to  $\rho < 0.8$ , where the optical depth is large. Moreover, significant optical depth differences between channels would reduce the gradients below the values from edge Thomson scattering. (Some

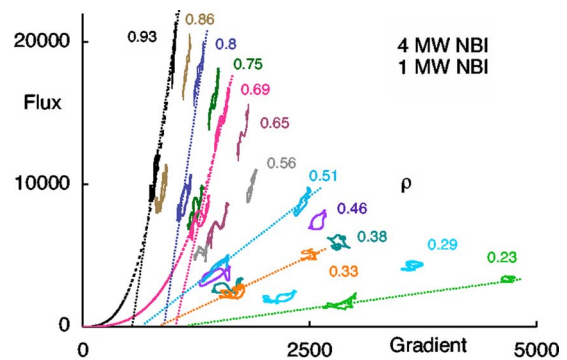


FIG. 6. (Color online) Electron heat flux (per particle) as a function of temperature gradient over a cycle of ECH modulation for the conditions of Fig. 1 and a second discharge with only 1 MW of NBI but otherwise identical. The dotted lines are linear fits; the dashed lines are power-law fits.

discharges with lower density have optical depths below 1 and clear errors in the outer ECE channels. These radii are omitted from the analysis.) Similar trajectories are also seen in *H* mode discharges, for which the optical depth is large everywhere. Conventional power balance transport analyses generally find that  $\chi_e$  rises sharply toward the edge, plausibly related to this result, but the analysis often stops short of the edge because the profiles are not well measured in this region. Such errors affect the position of the trajectory on the  $Q_e$  vs  $\nabla T_e$  plot, but they do not affect the trajectory because the quantities with poorly known absolute values are known to have no significant modulation.

Given the limited parameter range over which  $Q_e(\nabla T_e)$  is measured, one cannot uniquely determine the analytic form. Among the possibilities are a critical gradient or critical scale length corresponding to the extrapolation of the line segment to  $Q=0$  as well as a nonlinear form  $(\nabla T_e)^\alpha$  with  $\alpha$  in the range of 2–4.

This lack of uniqueness is confirmed in Fig. 6, which includes the trajectories from Fig. 5 as well as those from a similar discharge but with only 1 MW of neutral beam heating. Figure 6 includes the linear extrapolations to  $Q=0$  as well as  $(\nabla T_e)^3$  fits for  $\rho=0.93$  and  $\rho=0.69$ . However, one cannot argue that the trajectories of Fig. 6 represent the analytic form of  $Q_e(\nabla T_e)$ . The interpretation of trajectories in Fig. 5 as  $Q_e(\nabla T_e)$  is reasonable because only  $T_e$  changes over the modulation cycle, but the trajectories in Fig. 6 at different beam powers represent  $Q_e(\nabla T_e)$  at different ion temperatures, etc. The flux  $Q_e$  is a function of many variables, although  $\nabla T_e$  should be dominant. This argument has been applied by Hoang *et al.*<sup>13</sup> to infer  $Q_e(L_{Te})$  from a sequence of equilibria with increasing auxiliary heating. The trajectories have steep slopes, especially toward the core.

An alternative variable to  $\nabla T_e$  is the inverse scale length,  $\nabla T_e/T_e$ , often normalized in the form  $R/L_{Te}$ . Figure 7 presents the results of Fig. 6 in this form. This is essentially a different way of presenting the  $Q_e(\nabla T_e, T_e)$ . Although the values of  $R/L_{Te}$  are typical of most tokamaks and scale length is a natural variable in some theories, the trajectories of Fig. 7 do argue for the choice of  $R/L_{Te}$ . There are many instances in which the slope of  $Q_e(R/L_{Te})$  is negative, and the use of  $R/L_{Te}$  does not simplify the plot. Since  $\nabla T_e$  is the

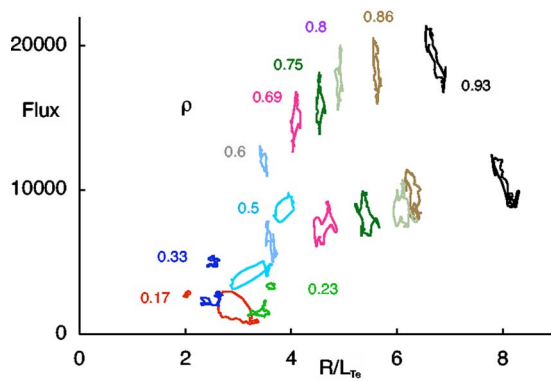


FIG. 7. (Color online) Electron heat flux (per particle) as a function of  $R/L_{Te}$ . Same conditions as in Fig. 6.

principal thermodynamic force driving the flux, it will be retained in subsequent plots of  $Q_e(\nabla T_e)$ . However, the critical thresholds will be shown as both  $\nabla T_e$  and  $R/L_{Te}$  below.

The experiment actually measures  $Q_e(\nabla T_e, T_e)$  along a specific path of  $\nabla T_e, T_e$ , which are the only quantities with significant modulation. A  $Q_e(T_e)$  or heat pinch cannot be excluded. Only an experiment that measured the flux for varying temperature while keeping the gradient constant would separate the pinch term. If the edge data were plotted as  $Q_e(T_e)$ , for example, to ascribe the transport to a convective velocity, the result would resemble the edge data of Fig. 5 quite closely. The trajectory would be steep with a slope of  $\sim 300$  m/s (outward) and extrapolate to a substantial offset, a sort of “critical temperature” for which the convective flux would be zero. Such large values of radial convective velocities are a non-negligible fraction of the sound speed and one hundred times typical particle convective velocities<sup>14</sup> as well as being oppositely directed.

A somewhat larger portion of  $Q_e(\nabla T_e)$  can be obtained with higher modulated ECH power, as shown in Fig. 8 for plasma conditions similar to those of Fig. 5 but with 1.5 MW of modulated ECH at a deposition radius of  $\rho=0.75$ . The results outside the deposition radius are an extension of those in Fig. 5, but the fraction of the plasma for which useful trajectories are obtained is smaller. The steep trajectories in the outer region of the plasma are the consequence of two

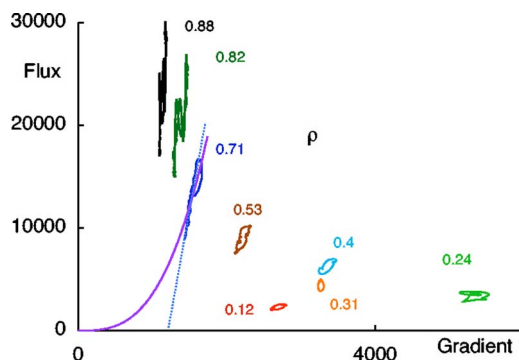


FIG. 8. (Color online) Electron heat flux (per particle) as a function of temperature gradient for the maximum modulated ECH power obtained in these experiments (1.5 MW). Deposition was at  $\rho=0.75$  into an  $L$  mode at 800 kA with 4 MW NBI and average density of  $2.5 \times 10^{19} \text{ m}^{-3}$ .

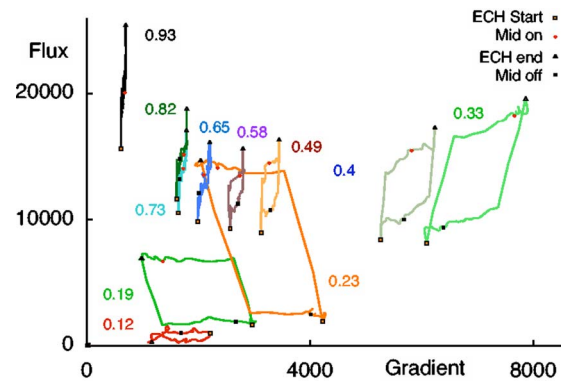


FIG. 9. (Color online) Electron heat flux (per particle) as a function of temperature gradient for 700 kW of modulated ECH power with deposition at  $\rho=0.2$  into an 800 kA discharge with 600 kW of continuous ECH power at  $\rho=0.3$  and average density of  $2.5 \times 10^{19} \text{ m}^{-3}$ .

robust features of the data. First, the system approaches an equilibrium rather rapidly on each half cycle (see Fig. 4); the added ECH power must therefore be removed by transport. Second, the changes in the edge parameters—temperature and gradient—are relatively small. In this case a 20% power modulation causes only a 10% temperature modulation and a 6% gradient modulation.

To obtain a better determination of  $Q_e(\nabla T_e)$  over the entire cross section, it is necessary to place the deposition radius near the center to modulate the flux everywhere. An example is shown in Fig. 9. After early beam heating to delay sawteeth, auxiliary heating was removed, and 0.7 MW of modulated ECH was applied at  $\rho=0.2$  with 1.2 MW of continuous ECH at  $\rho=0.3$  to maintain the electron temperature and slow the current penetration. Outside  $\rho=0.6$ , the trajectories look like those of Figs. 5, 6, and 8, but inside of that,  $Q_e(\nabla T_e)$  appear multivalued. Since the modulated ECH perturbation is fractionally significant in this case, a full analysis accounting for moving flux surfaces and modulation of the Ohmic and electron-ion power terms was employed. The multivalued property is associated with ECH power. The vertical segments occur rapidly at ECH switching; the horizontal segments represent the evolution with power on and power off. A similar sort of discontinuity with ECH power was reported by Stroth *et al.*<sup>15</sup> on the Wendelstein stellarator. The discontinuity is a consequence of the ECH power that must be accounted for. If the ECH power were reduced at the deposition radius, the local discontinuity would disappear, but that would not be consistent with the 0.7 MW which is observed in  $U(t)$ . To elucidate the matter, Fig. 10 shows a set of  $U(\rho, t)$  for this case, where the upper limit of the integral of Eq. (2) is  $\rho$ , not the full radius  $a$ . To make the modulation clearly visible, offsets have been applied for  $\rho < 1$ . One interpretation of Fig. 10 is that the ECH power is more broadly deposited than the codes predicted. The discontinuity in the derivatives at the switching times is generally taken as the indication of power deposition. The peak power density is certainly maximum near the deposition radius of 0.2, but much of the power is spread over most of the minor radius with a low-power density. If one assumes such a power deposition profile, Fig. 11 shows the resulting  $Q_e(\nabla T_e)$ . The

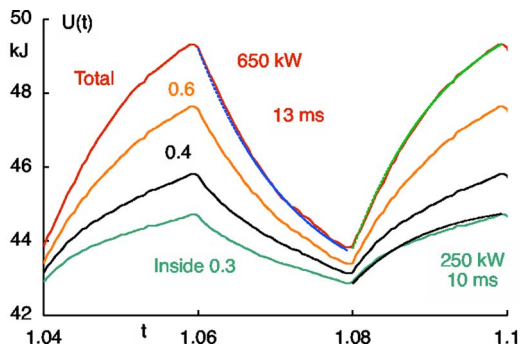


FIG. 10. (Color online) Electron energy  $U(t)$  for several radii for the discharge of Fig. 9. Offsets have been applied for all  $\rho < 1$  to retain a scale that shows  $\Delta U$ .

multivalued features are removed. The trajectories are again very steep near the edge and retain a “critical gradient” appearance for  $\rho > 0.4$ . Further in, the trajectories are consistent with diffusion,  $1 \leq \chi_e \leq 2$ , except in the core,  $\rho < 0.2$ . There, the flux appears independent of gradient, but the fluxes are small and the errors significant. Confinement may simply be very good in this region with actual fluxes nearly zero. Accurate central deposition would produce accurate results for  $\rho > 0.1$ , but transport very near the axis would be difficult to quantify with an ECH experiment.

Although the broadened deposition profile is not consistent with the TORAY calculation, direct measurements of the local power deposition in similar  $L$ -mode plasmas<sup>16</sup> have found profiles somewhat broader than predicted. For conditions very similar to these, almost half the total power was deposited outside the full width at half maximum (FWHM) about the peak. The apparent broadening was attributed to transport effects in Ref. 16. The implication of Fig. 9 is that transport is not an attractive explanation. The deposition profile used here is even broader than that shown in Ref. 16, but the low levels of power density required for the additional broadening may have been below the threshold for measuring significance in Ref. 16. Even if the experimental analyses are compatible, the conflict with code calculations of absorption remains to be explained. The fundamental wave physics

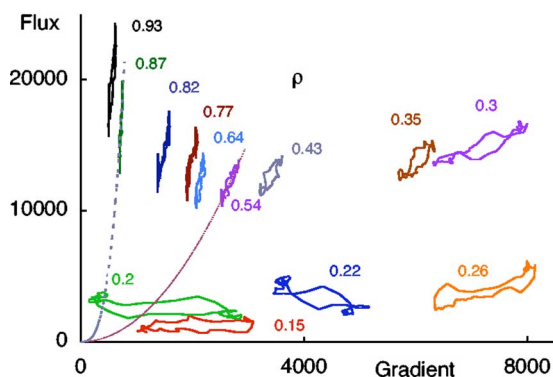


FIG. 11. (Color online) Electron heat flux (per particle) as a function of temperature gradient for the discharge of Fig. 9 with the modulated ECH power divided between the nominal resonant layer and a broader deposition at larger radii as suggested by Fig. 10. The dashed lines are power-law fits, cubic for  $\rho=0.87$  and quadratic for  $\rho=0.54$ .

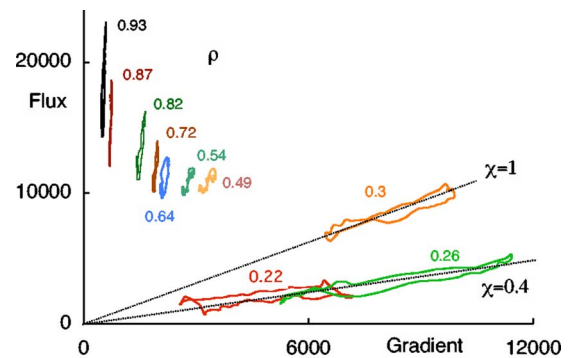


FIG. 12. (Color online) Electron heat flux (per particle) as a function of temperature gradient for an 800 kA Ohmic discharge with average density of  $2.5 \times 10^{19} \text{ m}^{-3}$  and modulated ECH at  $\rho=0.2$  and  $\rho=0.3$ , applied out of phase.

seems well established, but the antenna pattern or polarization may differ from those used in the code.

To increase the range of  $\nabla T_e$  in the trajectory, modulated ECH was applied at two radial locations, out of phase. The results are shown in Fig. 12 for an Ohmic target plasma and deposition at  $\rho=0.2$  and  $0.3$ , with somewhat more power applied at the larger radius. This case has been described and analyzed extensively by DeBoo *et al.*<sup>17</sup> with conventional Fourier techniques. They found no evidence of nonlinearity or crossing of a critical gradient despite the large change in gradient and gradient scale length. The results of Fig. 12 are entirely consistent with those conclusions. The trajectories in the deposition region,  $\rho \sim 0.25$ , are nearly diffusive and would imply a normal linear response. The fact that  $\chi$  is increasing rapidly with radius in this region is also consistent with the observation in Ref. 17 that a simple constant- $\chi$  model had to invoke jumps in  $\chi$  to fit the data. The trajectories for  $\rho \geq 0.5$  are similar to previous cases. Near  $\rho \sim 0.25$ ,  $\nabla T_e$  varies widely with little change in  $T_e$ . The experiment measures  $Q_e(\nabla T_e)$  explicitly.

As stated earlier, the segments of  $Q_e(\nabla T_e)$  in the outer portion of the plasma could be described by either a critical gradient and a  $\chi_{\text{inc}}$  for the slope or a form  $\kappa(\nabla T_e)^\alpha$ . However, the value of  $\alpha$  for a satisfactory fit varies with radius from 2 to greater than 3 over the range of cases, as illustrated again in Fig. 11. Since this sort of variation in the exponent does not arise in theories in a natural manner, it seems preferable to adopt the critical gradient description and search for the determinants of the critical gradient and  $\chi_{\text{inc}}$ , even though efforts to observe the critical gradient directly, e.g., Ref. 14, have proved unsuccessful. As is clear from the flux-gradient plots, the transition at the critical gradient only occurs at a point of zero flux, a condition difficult to realize in experiments, although Ryter *et al.*<sup>18</sup> have combined equilibrium and modulation experiments to infer a transition in  $\chi$  at a critical gradient in Ohmic discharges. Jacchia *et al.*<sup>19</sup> also favor a critical  $L_{T_e}$  formulation based on modulated ECH and cold pulse experiments and also require high values of  $\chi_{\text{inc}}$  toward the edge. The experimental results are collected in Figs. 13 and 14, which show values of  $\chi_{\text{inc}}$  and  $\nabla T_{\text{threshold}}$  as a function of radius for all conditions analyzed. The data span a limited range of central density, from 2 to 4

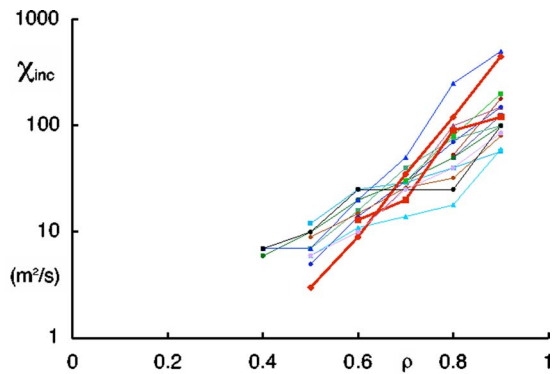


FIG. 13. (Color online) The incremental  $\chi$  [slope of  $Q_e(\nabla T_e)$ ] as a function of normalized minor radius for various conditions. The bold lines are  $H$  modes; the others are  $L$  modes.

$\times 10^{19}/\text{m}^3$ , and plasma current, 0.8 to 1.2 MA, with corresponding edge  $q$  values from 5 to 7. The range of electron and ion temperatures is quite large, with edge electron temperatures changing by a factor of 10 between some low-power cases and the  $QH$  mode, and  $T_e/T_i$  ranging from much less than 1 in the  $QH$  mode to much greater than 1 in ECH-only cases. The plots also include one set of values obtained from a sawtoothing  $L$ -mode discharge, not modulated ECH, but the result is notable only for being indistinguishable from the ECH values.

The most consistent and universal feature in the results is the increase in  $\chi_{\text{inc}}$  with radius. This strong, seemingly geometric, increase is difficult to attribute to changes in local plasma parameters. The strongest radial variation is temperature, yet high values of  $\chi_{\text{inc}}$  persist at the edge for high temperatures typical of much lower values of  $\chi_{\text{inc}}$  in the interior for other cases. High edge values of  $\chi_{\text{inc}}$ , decreasing by factors of 10–100 and merging to normal diffusive behavior at some  $\rho < 0.5$ , is a description consistent with all the observations. The apparent threshold temperature gradient, obtained by linear extrapolation of  $Q_e(\nabla T_e)$  to  $Q=0$  as in Figs. 6 and 8, is shown in Fig. 14 in units of eV ( $dT/d\rho$ ). At the edge, there is a general increase of the threshold with temperature. The thresholds in the  $QH$  mode, which has the highest temperature, are the highest, but the ELMy  $H$  mode

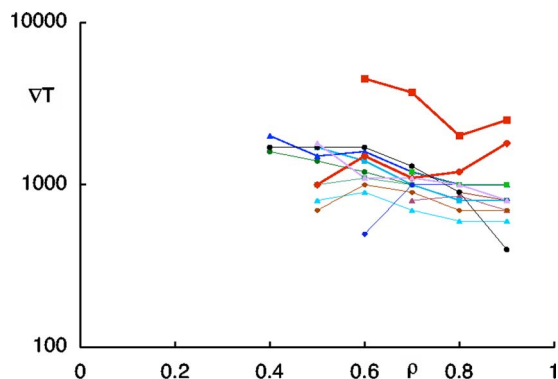


FIG. 14. (Color online) The critical gradient  $dT_e/d\rho$  (eV) as a function of normalized minor radius for various conditions. The bold lines are  $H$  modes, with the  $QH$  mode being the higher and the lower being ELMy; the others are  $L$  modes.

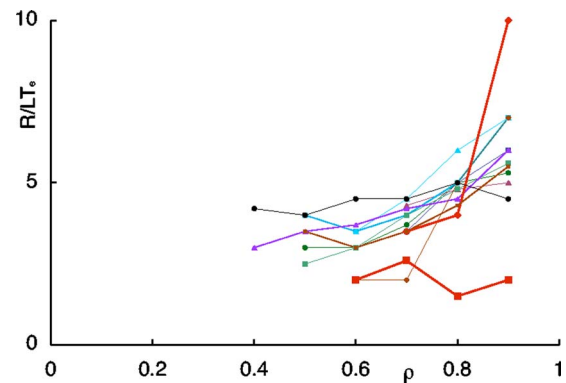


FIG. 15. (Color online) The critical scale length  $R/LT_e$  as a function of normalized minor radius for various conditions. The bold lines are  $H$  modes, with the  $QH$  mode being the lower and the high edge value being ELMy; the others are  $L$  mode.

has significantly higher temperatures than the remaining cases without correspondingly higher thresholds. A straightforward regression analysis gives a best-fit temperature dependence of  $T^{0.6}$ , but with considerable scatter. Other parameters are clearly important. Furthermore, the critical temperature gradient is only part of the picture. One needs a proper theory of the complete  $Q_e(\nabla T_e)$ . For comparison, the thresholds are expressed as  $R/LT_e$  and shown in Fig. 15. The thresholds for the  $QH$  mode are among the lowest because the temperatures are elevated more than the gradients. The ELMy  $H$  mode has the highest critical scale length at the edge because the large  $H$ -mode edge gradient occurs at a lower edge temperature with ELMs.

## V. CONCLUSIONS

Modern diagnostics make modulated ECH a more powerful technique for measuring electron thermal transport. One can determine  $Q_e(\nabla T_e)$ , at least over a range of  $Q_e$  and  $\nabla T_e$  near equilibria, which is appropriate for comparison with theoretical calculations. Although the segment of  $Q_e(\nabla T_e)$  is well determined experimentally, that is not sufficient to prescribe a unique functional form for  $Q_e(\nabla T_e)$ . The results are most easily described by a critical gradient model in which the stiffness ( $\chi_{\text{inc}}$ ) increases strongly with minor radius to high values at the edge. The critical gradient generally increases with electron temperature, but it has a complex functional dependence that could not be extracted from these experiments. The definitive comparison with theory would have to be based on calculations of  $Q_e(\nabla T_e)$  for values accessible in experiment.

## ACKNOWLEDGMENT

This work was supported by the U.S. Department of Energy under Grant No. DE-FG03-97-ER54415.

- <sup>1</sup>N. J. Lopes Cardozo, Plasma Phys. Controlled Fusion **37**, 799 (1995).
- <sup>2</sup>J. C. DeBoo, J. E. Kinsey, R. Bravenec, E. Fredrickson, C. M. Greenfield, Y. R. Lin-Liu, J. Lohr, T. C. Luce, G. R. McKee, R. Prater, C. L. Rettig, D. P. Schissel, G. M. Staebler, and R. E. Waltz, Nucl. Fusion **39**, 1935 (1999).

- <sup>3</sup>F. Ryter, G. Tardini, F. DeLuca, H. -U. Fahrbach, F. Imbeaux, A. Jacchia, K. K. Kirov, F. Leuterer, P. Mantica, A. G. Peeters, G. Pereverzev, and W. Suttrop, *Nucl. Fusion* **43**, 1396 (2003).
- <sup>4</sup>S. Cirant, G. Bracco, A. Bruschi, P. Buratti, F. DeLuca, B. Esposito, F. Gandini, E. Giovannozzi, G. Granucci, A. Jacchia, E. Lazzaro, E. Minardi, S. Nowak, G. Ramponi, C. Sozzi, and O. Tudisco, *Nucl. Fusion* **43**, 1384 (2003).
- <sup>5</sup>X. L. Zou, G. Giruzzi, J. F. Artaud, F. Bouquey, A. Clemencon, C. Darbos, R. J. Dumont, C. Guivarch, M. Lennholm, R. Magne, and J. L. Segui, *Nucl. Fusion* **43**, 1411 (2003).
- <sup>6</sup>M. E. Austin and J. Lohr, *Rev. Sci. Instrum.* **74**, 1457 (2003).
- <sup>7</sup>H. E. St. John, T. S. Taylor, Y. R. Lin-Liu, and A. D. Turnbull, *Proceedings of the 15th IAEA Conference, Seville, 1994* (IAEA, Vienna, 1994), Vol. 3, p. 603.
- <sup>8</sup>R. Prater, *Phys. Plasmas* **11**, 2349 (2004).
- <sup>9</sup>A. H. Kritiz, H. Hsuan, R. C. Goldfinger, and D. B. Batchelor, *Proceedings of the Third International Symposium on Heating in Toroidal Plasmas, Grenoble, Italy, 1982* (ECE Brussels, 1982), Vol. 2, p. 707.
- <sup>10</sup>J. L. Luxon, *Nucl. Fusion* **42**, 614 (2002).
- <sup>11</sup>J. Lohr, R. W. Callis, J. L. Doane, R. A. Ellis, Y. A. Gorelov, K. Kajiwara, D. Ponce, and R. Prater, *Proceedings of the 15th Topical Conference on Radio Frequency Power in Plasmas, Moran, Wyoming*, edited by C. B. Forest (AIP, New York, 2003), p. 335.
- <sup>12</sup>K. W. Gentle, M. E. Austin, and P. E. Phillips, *Phys. Rev. Lett.* **91**, 255001 (2003).
- <sup>13</sup>G. Hoang, C. Bourdelle, X. Garbet, G. Giruzzi, T. Aniel, and M. Ottaviani, *Phys. Rev. Lett.* **87**, 125001 (2001).
- <sup>14</sup>K. W. Gentle, O. Gehre, and K. Krieger, *Nucl. Fusion* **32**, 217 (1992).
- <sup>15</sup>U. Stroth, L. Giannone, and H.-J. Hartfuss, *Plasma Phys. Controlled Fusion* **38**, 611 (1996).
- <sup>16</sup>C. C. Petty, J. S. deGrassie, R. W. Harvey, Y. R. Lin-Liu, J. M. Lohr, T. C. Luce, M. A. Makowski, Y. A. Omelchenko, and R. Prater, *Proceedings of the 14th Topical Conference on Radio Frequency Power in Plasmas*, edited by T. K. Mau and J. deGrassie (AIP, New York, 2001), p. 275.
- <sup>17</sup>J. C. DeBoo, S. Cirant, T. C. Luce, A. Manini, C. C. Petty, F. Ryter, M. E. Austin, D. R. Baker, K. W. Gentle, C. M. Greenfield, J. E. Kinsey, and G. M. Staebler, *Nucl. Fusion* **45**, 494 (2005).
- <sup>18</sup>F. Ryter, F. Imbeaux, F. Leuterer, H. -U. Fahrbach, and W. Suttrop, *Phys. Rev. Lett.* **86**, 5498 (2001).
- <sup>19</sup>A. Jacchia, F. DeLuca, F. Ryter, A. Bruschi, F. Leuterer, R. Neu, G. Pereverzev, W. Suttrop, and D. Wagner, *Nucl. Fusion* **45**, 40 (2005).